Hindawi
Journal of Sensors
Volume 2019, Article ID 6739643, 9 pages
https://doi.org/10.1155/2019/6739643

Research Article

Dynamic Linear Predictive Optimization of Flexible Robot Profiling MFA Model

FengJun Hu, JianWei Lin, and HanJie Gu

Institute of Information Technology, Zhejiang Shuren University, Hangzhou, Zhejiang 310014, China

Correspondence should be addressed to FengJun Hu; jainism@msn.com

Received 17 January 2019; Revised 19 April 2019; Accepted 7 May 2019; Published 16 June 2019

Academic Editor: Antonio Lazaro

As the airbag of a flexible robot is affected by external environmental factors during the profiling process, there are many uncertainties in the process of deformation of the airbag. For this reason, the general nonlinear control strategy cannot obtain an accurate data model. In this paper, a flexible robot profiling MFA (Model-Free Adaptive) model based on adaptive predictive dynamic linear optimization is proposed. Firstly, the real-time thickness of the airbag is obtained through edge detection by using the image processing algorithm. Secondly, the airbag aerodynamic model is constructed by visual servo control strategy. Then, a nonlinear control system based on model-free adaptive control is established. Thirdly, the weighting factor is used to limit the variation range of the input quantity, and the deviation of the actual value and the expected value is corrected by the adaptive prediction mechanism. Finally, the servo control the airbag is completed. The experimental results show that the improved model proposed in this paper solves the overshoot phenomenon of the standard control model with less control error and higher robustness.

1. Introduction

In the profiling process of flexible robots, the profiling effect can be affected by external temperature, atmospheric pressure, airbag fabric material, and mutual extrusion degree [1–4]. In view of its nonlinear characteristics, the most commonly used control is PID control, but there is still a problem of low control accuracy. With the continuous development of computer vision technology, visual feedback servo control technology is used by more and more experts and scholars to control nonlinear systems with its characteristics of fast response, stability, and robustness [5–8].

Experts and scholars at home and abroad have already had some researches on robot profiling control. In [9], a flexible robot control method based on cross-section deformation is studied. Different cross-sections are established by inertia matrix and calculus to control the end-effector of the flexible robot. In [10], a profiling control method based on model prediction is proposed. The dynamic filter is used to correct the profiling precision, and the interpolation operation is used to ensure the stability and feasibility. In [11], a flexible robot control strategy based on STIFF-FLOP is introduced. The objective function is used for weighted learning, and the strategy is optimized in the strategy parameter space. In [12], a stochastic optimal control method for high-order cost statistics is proposed. For the setting of the factors with nonlinear dynamics and multiple uncertainties, the solution of a local optimal risk sensitivity and cost accumulation is introduced. In [13], a flexible robot facial profiling control strategy based on visual feedback interaction is designed. The artificial neural network (ANN) and Kinect sensor are used to identify the face, and the contour of the facial detail is controlled by the actuator. In [14], a genetic algorithm-based robot profiling control method is proposed. The genetic algorithm is used to find the angle mapping transformation matrix of a robot end effector and define the position and movable range of each actuator to realize profiling control. In [15], a new method for real-time robot profiling control is introduced. The Kinect vision sensor is used to collect the real-time status of the robot's profiling, and the inertial sensor is used to real-time control the robot's end effector. Reference [16] proposed a multiballoon visual servo control scheme, which directly controls the change of the target shape through the PID strategy and can provide higher control

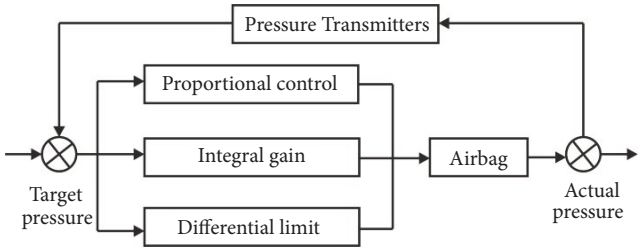

Figure 1: Incremental PID control strategy.

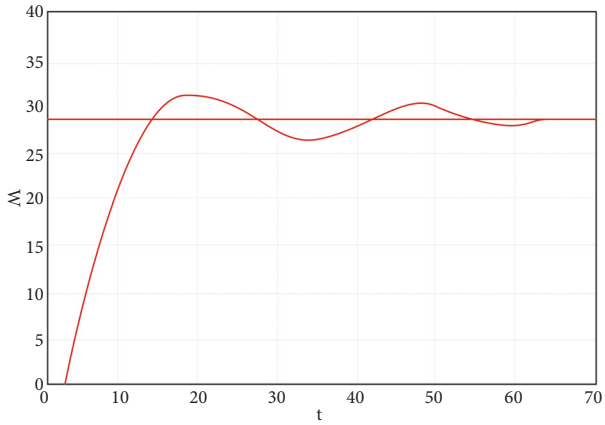

Figure 2: Simulation of incremental PID control.

precision than the traditional control scheme with intrabag air feedback. In [17], a robotic profiling control strategy based on steady-state genetic algorithm is proposed. The shape of the robot is measured by a 3D image sensor. The selection, variation, and evolution of the crossover operator are performed by the steady-state genetic algorithm (SSGA). Then, the deformation process performs adaptive search iterations to improve control accuracy.

The above methods and models are only applicable to the end effector of the flexible robot. Since the charge and discharge control of the flexible airbag robot has the characteristics of nonlinearity and uncertainty, the above-mentioned method cannot be applied to the control environment of the airbag flexible robot. For the quantitative control of nonlinear systems, model-free adaptive control is a suitable method, but there are few studies on this area. In [16], MFA model is introduced based on PID control algorithm. Yet there is still overshoot in the control of airbag inflation process, which reduces the control accuracy. Therefore, this paper proposes a flexible robot profiling MFA model based on adaptive predictive dynamic linear optimization, which can realize the real-time control of airbag charging and discharging deformation profiling of flexible robot.

2. Incremental PID Control Analysis

At present, the commonly used flexible robot airbag control method is incremental PID control [18, 19]. According to the relationship between the air intake volume and the air pressure inside the airbag, also the relationship between the air pressure inside the airbag and the airbag volume, a negative feedback closed loop system is constructed. In order to improve the accuracy, the airbag pressure and volume deviation are continuously detected through the proportional control link.

In the airbag inflation control, the general PID control algorithm will have steady-state deviation under steady-state conditions. Therefore, in order to avoid this problem, the incremental PID control algorithm optimizes the low-frequency gain through the integral link, and limits the control by the predicted value of the error differential. Thus, the deviation under steady-state condition can be reduced. The airbag control method based on incremental PID control is shown in Figure 1.

The simulation of the above mentioned method is shown in Figure 2.

Where, the x-coordinate is time and the y-coordinate is pressure (cmHg) in the air bag.

It can be seen from the simulation results that the incremental PID control method has a certain amount of overshoot, and certain fluctuations will occur in the set value interval, which will greatly increase the workload of the valve during gas charging and discharging process and reduce the system life.

3. Airbag Aerodynamic Model Based on Visual Servo Control

In order to improve the deformation accuracy of the airbag, this paper adopts the visual servo control system [20–22]

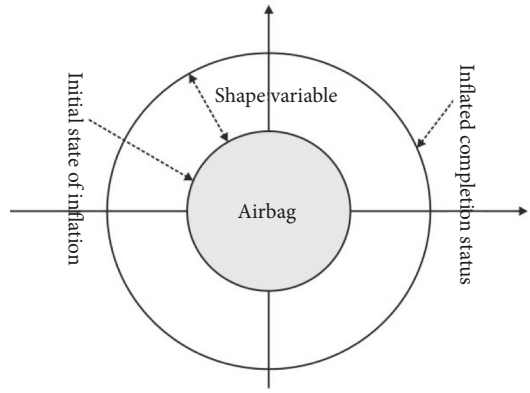

Figure 3: The deformation process of airbag inflation.

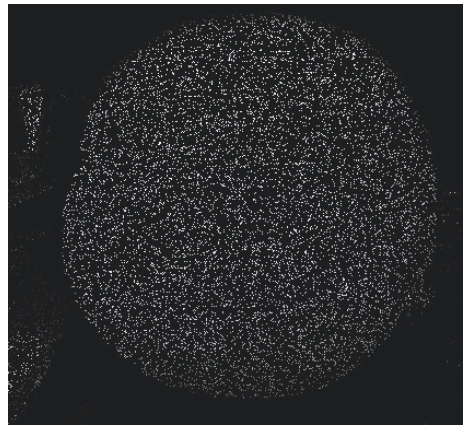

Figure 4: Edge detection result of the Roberts operator.

to retrieve the real-time information of the thickness of the flexible robot airbag. The deformation process of the airbag inflation is show in Figure 3.

In this paper, the Roberts operator is used for edge detection [23–25]. Let the grayscale of the image on the coordinate (x, y) be $f(x, y)$, then, the spatial 1st-order differential is as follows:

$$\nabla f(x, y) = \frac{\partial f(x, y)}{\partial x} n_x + \frac{\partial f(x, y)}{\partial y} n_y \tag{1}$$

where the unit vector in the directions of x, y is n_x, n_y, respectively.

By differentially expressing x, y, the edge intensity value can be obtained:

$$\left|\nabla f(x, y)\right| = \sqrt{f_x^2(x, y) + f_y^2(x, y)} \tag{2}$$

And the edge detection result of the Roberts operator (Figure 4) is shown in

$$G(x, y) = \sqrt{\left[f(x+1, y+1) + f(x, y) + \delta\right]^2 + \left[f(x+1, y) + f(x, y+1) + \delta\right]^2} \tag{3}$$

where (x, y) is the pixel coordinate value in the image and $f(x, y)$ is the gray value of the pixel point, $G(x, y)$ is the edge detection strength, and δ is the modified value of gasbag morphology change.

Through the result obtained by the Roberts operator, the position of the airbag can be known. When the center point of the airbag remains unchanged, the distance between the edge value with the maximum distance from the center point and the center point is the real-time thickness value of the airbag.

The real-time thickness value of the airbag obtained above is used as a basis for the control of charging and discharging process to construct airbag aerodynamic model based on visual servo control, which is shown in Figure 5.

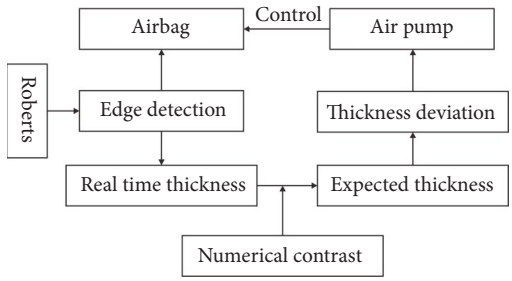

Figure 5: Airbag aerodynamic model based on visual servo control.

Thus, the airbag aerodynamic model based on visual servo control can be expressed as follows:

$$y(k+1) = y(k) + \eta(k) \tag{4}$$

where $y(k+1)$ is the output pressure value, k is the real-time airbag thickness value obtained by Roberts operator, and $\eta(k)$ is the deviation from the expected thickness value.

4. Dynamic Linear Model-Free Control of Adaptive Prediction

Due to changes in external temperature, atmospheric pressure, airbag fabric material, and mutual extrusion degree, the deformation of the airbag will be affected. Therefore, the above model has strong nonlinearity, and it must be quantized to achieve best control. In order to overcome the shortcomings of the incremental PID control algorithm mentioned above, this paper introduces the Model-Free Adaptive (MFA) method to control the charging and discharging of the airbag.

4.1. Dynamic Linearization of MFA Model. According to the airbag aerodynamic model based on visual servo control, a nonlinear control system based on model-free adaptive control is constructed, which is shown in

$$\begin{aligned} &y(t+1) \\ &\quad = f\left(y(t), \ldots, y\left(t-n_y\right), e(t), \ldots, u\left(t-n_u\right)\right) \end{aligned} \tag{5}$$

where $y(t)$, $e(k)$ expresses the output and input of the system pressure at time t, respectively. n_y, n_u is unknown order of the system, respectively, and $f(\cdot)$ is nonlinear function with unknown airbag parameters.

If the above nonlinear control system meets $|\Delta y(t+1)| \le a|\Delta e(t)|$, and $\Delta e(t) \neq 0$, the following can be obtained according to Cauchy's mean value theorem of differential:

$$\Delta y(t+1) = \frac{\partial f}{\partial e(t)} \Delta e(t) + f \tag{6}$$

where $\partial f / \partial e(t)$ is the partial derivative on n_y variables of nonlinear function $f(\cdot)$.

Then, the result of dynamic linearization can be shown in

$$\Delta y(t+1) = \varphi(t) \Delta e(t) \tag{7}$$

where $\varphi(t)$ is pseudo gradient vector.

In order to control the dynamic linearization of the nonlinear system of formula (7) within a reasonable range, $\Delta e(t)$ must be limited.

Assuming the output value of the airbag pressure at any time t is $y^*(t)$. In order to approach the expected value as close as possible, it is necessary to obtain the optimal $\Delta e(t)$ and limit its range, so as to avoid the system instability caused by excessive input value.

Therefore, a quadratic index function is introduced.

$$\begin{aligned} J(\Delta e(t)) &= \left\| y^*(t+1) - y(t+1) \right\|^2 \\ &\quad + \lambda \left\| e(t) - e(t-1) \right\|^2 \end{aligned} \tag{8}$$

where λ is the weighting factor; it can control the range of $\Delta e(t)$; the smaller is the weighting factor, the less restriction is on $\Delta e(t)$, which can cause the system to oscillate. Thus, formula (7) can be changed to the following:

$$y(t+1) = y(t) + \varphi(t) \Delta e(t) \tag{9}$$

Put (9) into (8), and partial derivative can be obtained:

$$\begin{aligned} \frac{\partial J(\Delta e(t))}{\partial(\Delta e(t))} &= 2\left(\varphi(t) + \lambda\right) \Delta e(t) \\ &\quad - 2\varphi(t)\left(y^*(t+1) - y(t)\right) \end{aligned} \tag{10}$$

If the above formula is equal to 0, the variation of $\Delta e(t)$ is

$$\Delta e(t) = \frac{\varphi(t)\left(y^*(t+1) - y(t)\right)}{\lambda + \varphi(t)} \tag{11}$$

4.2. Control Model Optimization Based on Adaptive Prediction. On the basis of dynamic linearization, this paper also uses adaptive prediction mechanism to improve it. Let $y^*(t)$ be the expected output value at time t of the system, and let $\sigma(t)$ be the deviation between the expected output value and the actual value at time t.

Then, the following holds:

$$\sigma(k+1) = y^*(k+1) - y(k+1) \tag{12}$$

If $\Delta y(t+1) = \varphi(t) \Delta \sigma(t)$, we can obtain

$$\Delta \sigma(t) = \Delta y^*(t+1) - \varphi(t) \Delta e(t) \tag{13}$$

where $\Delta y^*(t+1)$ is the difference between output values at adjacent times.

Set sampling time as T; in this sampling time, the sum of deviations before time t is γ; then, the following is established:

$$\begin{aligned} \begin{bmatrix} \gamma(t+1) \\ \sigma(t+1) \end{bmatrix} &= \begin{bmatrix} 1 & T \\ 0 & 1 \end{bmatrix} \begin{bmatrix} \gamma(t) \\ \sigma(t) \end{bmatrix} + \begin{bmatrix} 0 \\ -\varphi(t) \end{bmatrix} \Delta e(t) \\ &\quad + \begin{bmatrix} 0 \\ 1 \end{bmatrix} \Delta y^*(t+1) \end{aligned} \tag{14}$$

Through the statistics and prediction of the deviation $\sigma(t)$, the error is corrected and neutralized; finally the control accuracy is improved.

Then, control input criterion function is optimized, and the following can be obtained:

$$J = \sum_{\alpha=1}^{N} \left(y\left(t+\alpha\right) - y^*\left(t+\alpha\right)\right)^2 + \lambda \sum_{\beta=0}^{N_\mu - 1} \Delta e^2\left(t+\beta\right) \quad (15)$$

where $y^*(t+\alpha)$ is the expected output value of the system at time $t+\alpha$, and $y(t+\alpha)$ is the actual output at time $t+\alpha$, λ is weighting factor.

Let $Y_N^*(t+1) = [y^*(t+1), y^*(t+2), \ldots, y^*(t+N)]^T$; the vector form of (15) can be expressed as

$$\begin{aligned} J &= \left[Y_N^*\left(t+1\right) - Y_N^*\left(t+1\right)\right]^T \left[Y_N\left(t+1\right) - Y_N^*\left(t+1\right)\right] \\ &\quad + \lambda \Delta R_{N_\mu}^T\left(t\right) \Delta R_{N_\mu}\left(t\right) \end{aligned} \quad (16)$$

where $\Delta R_N(t)$ is the control input vector of the system; this can be calculated as follows:

$$\Delta R_N\left(t\right) = \left[\Delta e\left(t\right), \Delta e\left(t+1\right), \ldots, \Delta e\left(t+N-1\right)\right]^T \quad (17)$$

By calculating the extremum of $\Delta R_N(t)$, the control quantity of the current time can be obtained:

$$e\left(t\right) = e\left(t-1\right) + g^T \Delta R_{N_\mu}\left(t\right) \quad (18)$$

where $g^T = [1, 0, \ldots, 0]^T$.

4.3. Dynamic Linear Model-Free Control of Adaptive Prediction. The implementation steps of the adaptive predictive dynamic linear model-free control strategy proposed in this paper are as follows.

Step 1. The image of the airbag is gained, and edge detection is carried out by Roberts operator; then, the real-time thickness of the airbag is obtained.

Step 2. The parameters of the airbag aerodynamic model are initialized, and the threshold range of the error is set.

Step 3. Limit the range of control input by $\lambda(e(t) - e(t-1))^2$.

Step 4. The deviation $\sigma(t)$ between the expected output value and the actual value at time t is calculated.

Step 5. The sum γ of the deviations before the time t is calculated; then, statistics and prediction of deviation $\sigma(t)$ can be made.

Step 6. By using the predicted value of the deviation, the control input value $e(t)$ at this moment can be obtained.

Step 7. The predicted output value $y(k+1)$ can be obtained by inputting the control input value $e(t)$ obtained at Step 6 into the airbag aerodynamic model.

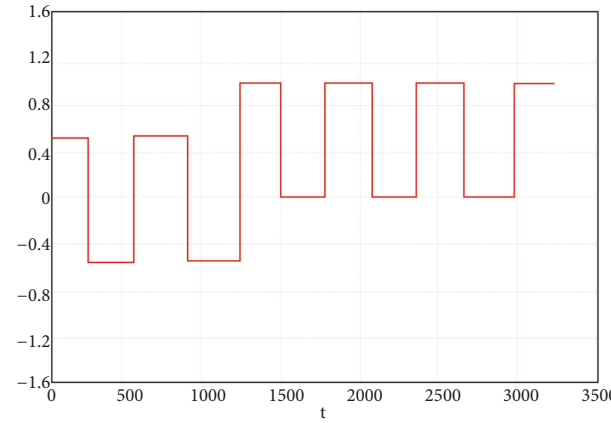

Figure 6: The output result of linear system.

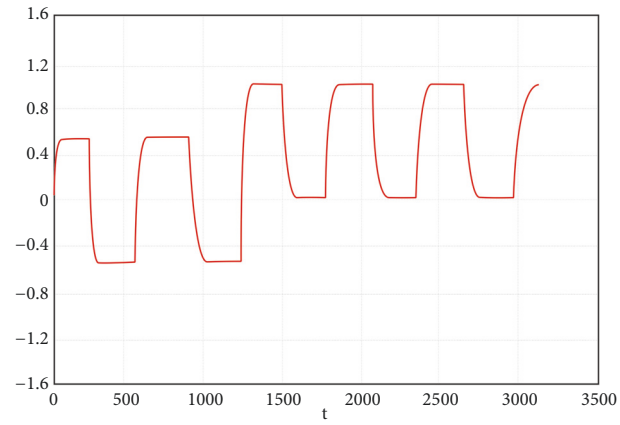

Figure 7: Simulation result of model-free adaptive control model with dynamic linearization.

Step 8. The airbag real-time thickness value gained at Step 1 is compared with the predicted output value $y(k+1)$; the deviation $\sigma(t)$ can be obtained.

Step 9. Repeat until the deviation is less than the set threshold.

5. Simulations and Analysis

5.1. Dynamic Linearization Model Simulation. A model-free adaptive control model with dynamic linearization is constructed and simulated by a linear system and a nonlinear system. The linear system is shown in (19) and the output curve is displayed in Figure 6.

$$y\left(k+1\right) = \begin{cases} 0.02y\left(k-30\right) + 0.15u\left(k - \dfrac{8}{15}\right) \\ -0.2y\left(3k-5\right) + 0.04u\left(k-2\right) \end{cases} \quad (19)$$

where u and k are parameter variables of the linear system.

y is the expected target value and in the figure is the ordinate value (the same as in Figure 7).

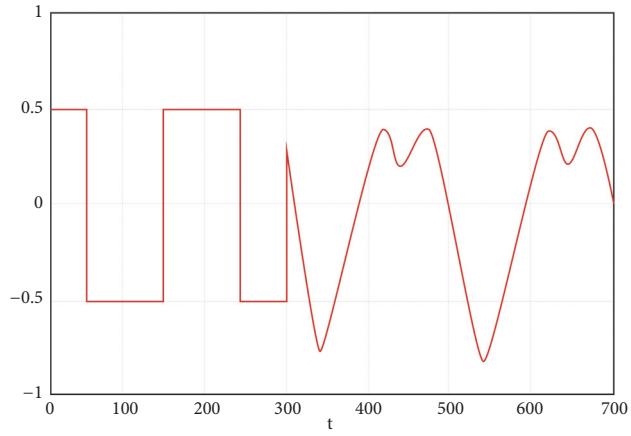

Figure 8: The output result of nonlinear time-varying system.

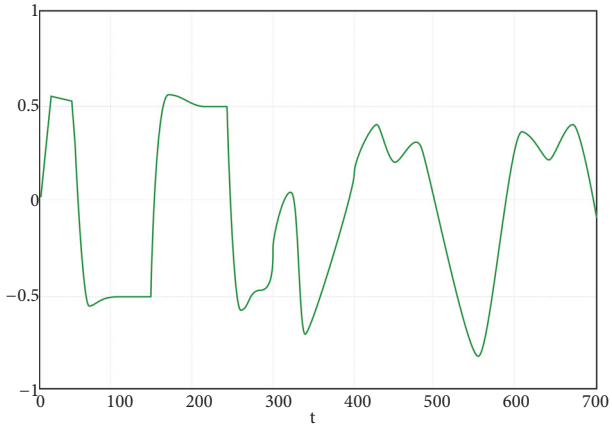

Figure 9: Simulation result of model-free adaptive control model with dynamic linearization.

The simulation results of model-free adaptive control model with dynamic linearization are shown in Figure 7.

As can be seen from Figures 6 and 7, for this linear system, the model-free adaptive control model with dynamic linearization has better control accuracy and smaller deviation from the expected value.

The nonlinear time-varying system is shown in (20), and the output curve is displayed in Figure 8.

$$y(k+1) = \begin{cases} \dfrac{y(k)}{1+y^2(k)} + u^3(k), & k \le 500 \\ \dfrac{y(k)\,y(k-1)\,y(k-2)\,u(k-1)\left(y(k-2)-1\right) + a(k)\,u(k)}{1+y^2(k-1)+y^2(k-2)} \end{cases} \tag{20}$$

where, u and k are parameter variables of the nonlinear system.

y is the expected target value and in the figure is the ordinate value (the same as in Figure 9).

The simulation results of model-free adaptive control model with dynamic linearization are shown in Figure 9.

By comparing Figures 8 and 9, it can be found that the model-free adaptive control model with dynamic linearization has a good control effect on the nonlinear time-varying system. The output of the system varies with the expected output, and the deviation is small.

5.2. Adaptive Prediction Model Simulation. Although the model-free adaptive control model with dynamic linearization has better control effect from the above simulation results, its accuracy needs to be improved. Therefore, this paper carries out adaptive predictive optimization and implements modeling towards the established adaptive predictive

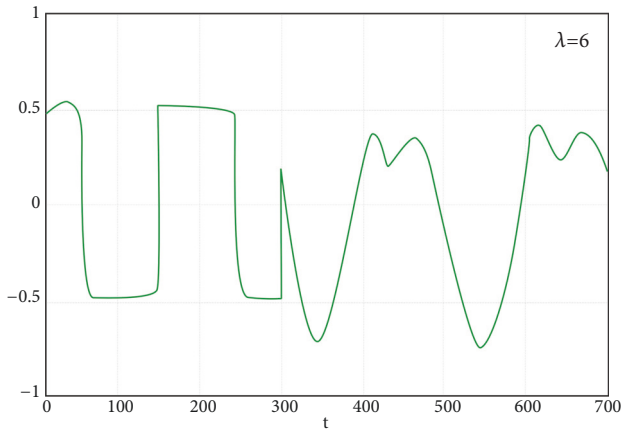

Figure 10: Output result of simulation.

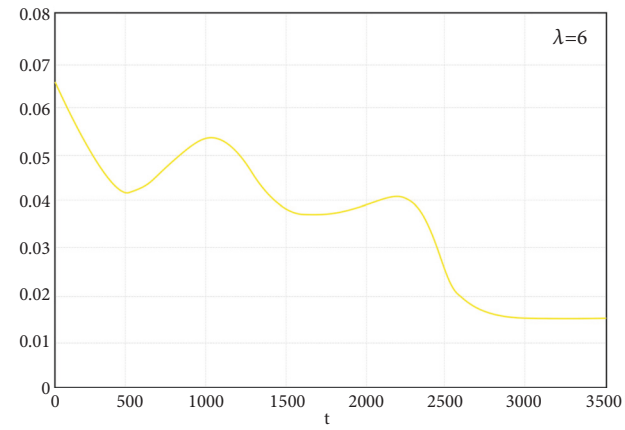

Figure 11: Relative control error.

dynamic linear model-free control method and simulates in the above-mentioned nonlinear system.

In this paper, since $\lambda(e(t) - e(t-1))^2$ is used to limit the range of control output value, the simulation comparison of different weighting factors λ is carried out.

When $\lambda = 2$, the simulation results are shown in Figures 12 and 13.

From the simulation results of Figures 10–13, it can be seen that the adaptive predictive dynamic linear model-free control method proposed in this paper has a good approximation effect on the set expected output value, and the error is small, which shows that its theory is feasible.

5.3. Flexible Robot Bag Deformation Control Simulation. A spherical balloon of flexible robot with diameter of 30cm and permeability coefficient of 0.008 is used to construct a charging and discharging control model. The airbag is controlled by the adaptive predictive dynamic linear model-free control model built above, where the input value is the air intake and the output value is the thickness of the airbag.

When $\lambda = 2$, the effect of model-free adaptive control is shown in Figures 14 and 15. When $\lambda = 6$, the effect of model-free adaptive control is shown in Figures 16 and 17.

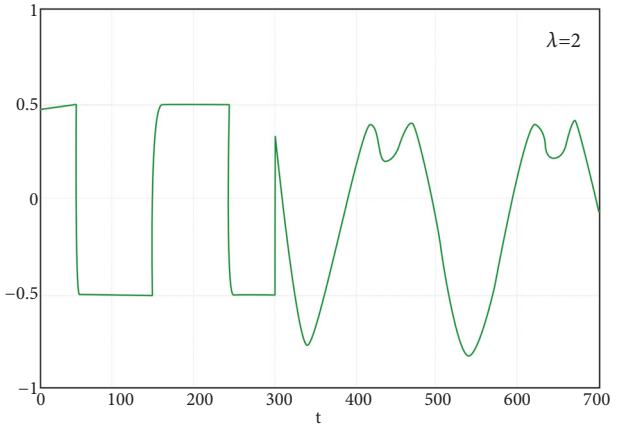

Figure 12: Output result of simulation.

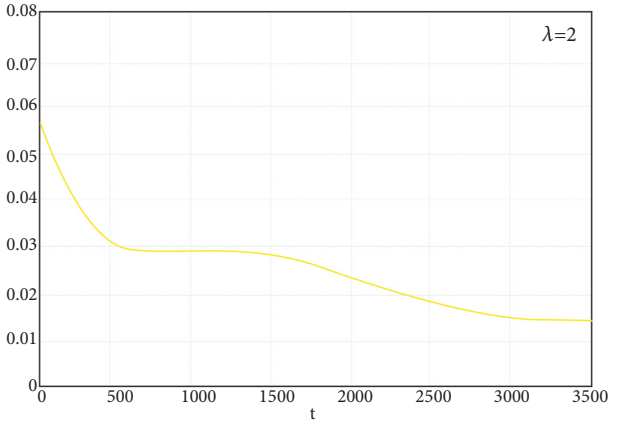

Figure 13: Relative control error.

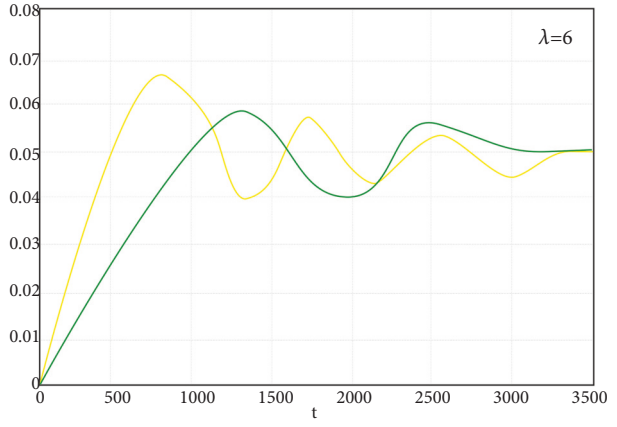

Figure 14: The airbag control output result.

In the figure, green is the standard model-free adaptive control algorithm and yellow is the adaptive predictive dynamic linear model-free control method proposed in this paper.

From Figures 14–17, it can be seen that, compared with the standard model-free adaptive control algorithm,

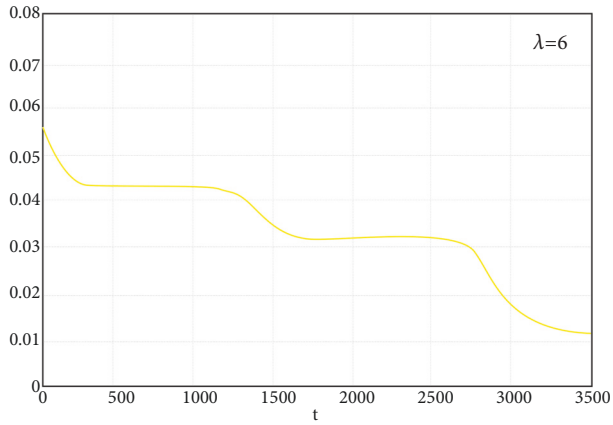

Figure 15: Airbag control relative error.

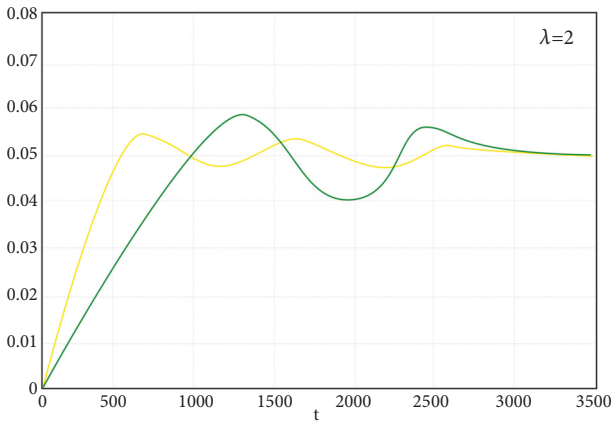

Figure 16: Airbag control output result.

the improved algorithm proposed in this paper has higher control accuracy, and the weight factor λ plays a certain role in restricting the control of the airbag. And when $\lambda = 2$, the control error is smaller.

6. Conclusions

For the multiballoon flexible robot profiling system, it is difficult to achieve good control in complex environment by using air pressure parameters as feedback control method. However, visual servo control method can directly control the change of target shape, and the control effect is better. In the aspect of control algorithm, the design of model-free adaptive controller does not depend on the precise mathematical model of the controlled system. The algorithm has fewer adjustable parameters and is compatible with different systems. In order to solve the problems existing in the control of the airbag charging and discharging process, a flexible robot airbag profiling control model based on adaptive predictive dynamic linear optimization is proposed. Simulations show that the proposed model is effective and the control error is small.

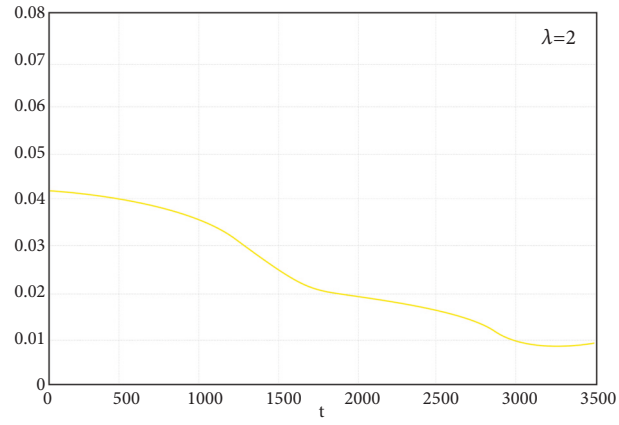

Figure 17: Airbag control relative error.

Data Availability

The data used to support the findings of this study are available from the corresponding author upon request.

Conflicts of Interest

The authors declare that they have no conflicts of interest.

Acknowledgments

This work was supported by the National Natural Science Foundation of China (Grant no. 51675490), the Department of Science and Technology of Zhejiang Province (Grant no. 2017C31050), the Department of Science and Technology of Zhejiang Province (Grant no. 2017C31063), and Young Academic Team Project of Zhejiang Shuren University.

References

[1] L. Bo and G. Shuyi, "Study of active airbag vent control technology," *Spacecraft Recover & Remote Sensing*, vol. 37, no. 3, pp. 39–47, 2016.

[2] W. Xiaodong, S. Lianguo, Z. Wei, and S. Rui, "Research on tension control system for automobile safety airbag folding machine," *Machine Tool & Hydraulics*, vol. 44, no. 11, pp. 109–112, 2016.

[3] F. Wang, J. Zhang, L.-R. Peng, and G.-W. Wang, "Motion-precision control in bonnet-polishing," *Optics and Precision Engineering*, vol. 23, no. 8, pp. 2220–2228, 2015.

[4] H. Jian, M. Jisheng, W. Dalin, D. Shijie, and S. Yezun, "Numerical simulation of airbag cushion process of landing," *Packaging Engineering*, vol. 36, no. 13, pp. 69–73, 2015.

[5] Q. Pu, S. Rui, L. Jinhong, and Y. Zhen, "Numerical simulation of multi-airbags buffer landing system," *Fire Control & Command Control*, vol. 40, no. 3, pp. 125–129, 2015.

[6] R. B. Timmers, R. C. Hardy, and J. V. Welch, "Modeling and simulation of the second-generation orion crew module airbag landing system," *Aiaa Journal*, vol. 5, pp. 225–230, 2009.

[7] B. Tutt, S. Gill, A. Wilson, and K. Johnson, "A summary of the development of a nominal land landing airbag impact

attenuation system for the orion crew module," *Aiaa Journal*, vol. 12, pp. 14–18, 2009.

[8] Z. Tianyuan, C. Libo, Z. Feitie, and W. Menghua, "Design of automotive airbag control system based on the power PC," *Application of Electronic Technique*, vol. 43, no. 10, pp. 63–66, 2017.

[9] L. Celentano, "Modeling of flexible robots with varying cross section and large link deformations," *Journal of Dynamic Systems, Measurement, and Control, Transactions of the ASME*, vol. 138, no. 2, 2016.

[10] A. Mukovskiy, C. Vassallo, M. Naveau, O. Stasse, P. Souères, and M. A. Giese, "Adaptive synthesis of dynamically feasible full-body movements for the humanoid robot HRP-2 by flexible combination of learned dynamic movement primitives," *Robotics and Autonomous Systems*, vol. 91(C), pp. 270–283, 2017.

[11] S. Calinon, D. Bruno, and M. S. Malekzadeh, "Human-robot skills transfer interfaces for a flexible surgical robot," *Computer Methods and Programs in Biomedicine*, vol. 116, no. 2, pp. 81–96, 2014.

[12] J. R. Medina and S. Hirche, "Considering uncertainty in optimal robot control through high-order cost statistics," *IEEE Transactions on Robotics*, vol. 34, no. 4, pp. 1068–1081, 2018.

[13] A. Meghdari, S. B. Shouraki, A. Siamy, and A. Shariati, "The real-time facial imitation by a social humanoid robot," *International Conference on Robotics & Mechatronics*, vol. 26, pp. 524–529, 2016.

[14] M. Nishiyama and H. Iba, "Applying conversion matrix to robots for imitating motion using genetic algorithms," *IEEE Congress on Evolutionary Computation*, vol. 6, pp. 938–944, 2014.

[15] A. Jha, S. S. Chiddarwar, and V. Alakshendra, "Motion Programming of scorbot ER-4u using fusion of robot kinematics and inertial sensor," *International Conference on CAD/CAM, Robotics and Factories of the Future*, vol. 10, pp. 263–273, 2016.

[16] C. Xing, H. Kuangrong, and D. Yongsheng, "Simulation of visual servo control for multi-aerocyst flexible fitting robot," *Computer Simulation*, vol. 31, no. 10, pp. 381–385, 2014.

[17] T. Obo, C. K. Loo, and N. Kubota, "Robot posture generation based on genetic algorithm for imitation," *IEEE Congress on Evolutionary Computation*, vol. 25, pp. 552–557, 2015.

[18] I. Carlucho, M. De Paula, S. A. Villar, and G. G. Acosta, "Incremental Q-learning strategy for adaptive PID control of mobile robots," *Expert Systems with Applications*, vol. 80, pp. 183–199, 2017.

[19] O. S. Bhatti, O. B. Tariq, A. Manzar, and O. A. Khan, "Adaptive intelligent cascade control of a ball-riding robot for optimal balancing and station-keeping," *Advanced Robotics*, vol. 4, pp. 1–14, 2017.

[20] S. Krupinski, G. Allibert, M.-D. Hua, and T. Hamel, "An inertial-aided homography-based visual servo control approach for (almost) fully actuated autonomous underwater vehicles," *IEEE Transactions on Robotics*, vol. 33, no. 5, pp. 1041–1060, 2017.

[21] P. Serra, R. Cunha, T. Hamel, D. Cabecinhas, and C. Silvestre, "Landing of a quadrotor on a moving target using dynamic image-based visual servo control," *IEEE Transactions on Robotics*, vol. 32, no. 6, pp. 1524–1535, 2016.

[22] A. Hajiloo and M. Keshmiri, "Robust online model predictive control for a constrained image-based visual servoing," *IEEE Transactions on Industrial Electronics*, vol. 63, no. 4, pp. 2242–2250, 2016.

[23] M. Kang, Q. Xu, and B. Wang, "A roberts' adaptive edge detection method," *Journal of Xi'an Jiaotong University*, vol. 42, no. 10, pp. 1240–1244, 2008.

[24] T. Banerjee and G. V. Moustakides, "Minimax optimality of shiryaev-roberts procedure for quickest drift change detection of a brownian motion," *Sequential Analysis*, vol. 36, no. 3, pp. 355–369, 2017.

[25] W. Yongge, H. Hongzhou, and L. Haiyang, "An improved image edge detection algorithm based on roberts and grey relational analysis," *Journal of Graphics*, vol. 35, no. 4, pp. 637–642, 2014.